Quinine

Agbo, Chinazom Precious; Ugwuanyi, Timothy Chukwuebuka; Eze, Osita Christopher; Onugwu, Adaeze Linda; Echezona, Adaeze Chidiebere; Nwagwu, Chinekwu Sherridan; Uzondu, Samuel Wisdom; Ogbonna, John Dike; Ugorji, Lydia Onyinyechi; Nnamani, Petra Obioma; Akpa, Paul Achile; Reginald-Opara, Joy Nneji; Ogbodo, John Onyebuchi; McConville, Christopher; Attama, Anthony Amaechi; Momoh, Mumuni Audu; Ofokansi, Kenneth Chibuzor

DOI:
10.3390/pr11061811

Document Version
Publisher's PDF, also known as Version of record

Citation for published version (Harvard):
Agbo, CP, Ugwuanyi, TC, Eze, OC, Onugwu, AL, Echezona, AC, Nwagwu, CS, Uzondu, SW, Ogbonna, JD, Ugorji, LO, Nnamani, PO, Akpa, PA, Reginald-Opara, JN, Ogbodo, JO, McConville, C, Attama, AA, Momoh, MA & Ofokansi, KC 2023, 'Quinine: Redesigned and Rerouted', *Processes*, vol. 11, no. 6, 1811. https://doi.org/10.3390/pr11061811

processes

MDPI

Article

Quinine: Redesigned and Rerouted

Chinazom Precious Agbo [1,2,*], Timothy Chukwuebuka Ugwuanyi [1], Osita Christopher Eze [3], Adaeze Linda Onugwu [1], Adaeze Chidiebere Echezona [1], Chinekwu Sherridan Nwagwu [1], Samuel Wisdom Uzondu [1], John Dike Ogbonna [1], Lydia Onyinyechi Ugorji [4], Petra Obioma Nnamani [1], Paul Achile Akpa [1], Joy Nneji Reginald-Opara [1], John Onyebuchi Ogbodo [5], Christopher McConville [2,*], Anthony Amaechi Attama [1,6], Mumuni Audu Momoh [1] and Kenneth Chibuzor Ofokansi [1]

[1] Drug Delivery and Nanomedicines Research Laboratory, Department of Pharmaceutics, University of Nigeria, Nsukka 410001, Enugu State, Nigeria; chukwuebuka.ugwuanyi.189655@unn.edu.ng (T.C.U.); adaeze.onugwu@unn.edu.ng (A.L.O.); adaeze.echezona@unn.edu.ng (A.C.E.); chinekwu.nwobi@unn.edu.ng (C.S.N.); samuel.uzondu@unn.edu.ng (S.W.U.); john.ogbonna@unn.edu.ng (J.D.O.); petra.nnamani@unn.edu.ng (P.O.N.); paul.akpa@unn.edu.ng (P.A.A.); joy.achuam@unn.edu.ng (J.N.R.-O.); anthony.attama@unn.edu.ng (A.A.A.); audu.momoh@unn.edu.ng (M.A.M.); kenneth.ofokansi@unn.edu.ng (K.C.O.)
[2] School of Pharmacy, College of Medical and Dental Sciences, University of Birmingham, Birmingham B4 6BN, UK
[3] Department of Pharmaceutical Microbiology and Biotechnology, Faculty of Pharmaceutical Sciences, University of Nigeria, Nsukka 410001, Enugu State, Nigeria; osy.eze@unn.edu.ng
[4] Department of Pharmaceutical Technology and Industrial Pharmacy, Faculty of Pharmaceutical Sciences, University of Nigeria, Nsukka 410001, Enugu State, Nigeria; lydia.ugorji@unn.edu.ng
[5] Department of Science Laboratory Technology, University of Nigeria, Nsukka 410001, Enugu State, Nigeria; john.ogbodo@unn.edu.ng
[6] Department of Pharmaceutics and Pharmaceutical Technology, Faculty of Pharmaceutical Sciences, Enugu State University of Science and Technology, Agbani, Enugu 400102, Enugu State, Nigeria
* Correspondence: chinazom.agbo@unn.edu.ng (C.P.A.); c.mcconville.2@bham.ac.uk (C.M.); Tel.: +234-8062275858 (C.P.A.); +44-701214143209 (C.M.)

Abstract: Quinine hydrochloride (QHCl) has remained a very relevant antimalarial drug 400 years after its effectiveness was discovered. Unlike other antimalarials, the development of resistance to quinine has been slow. Hence, this drug is to date still used for the treatment of severe and cerebral malaria, for malaria treatment in all trimesters of pregnancy, and in combination with doxycycline against multidrug-resistant malaria parasites. The decline in its administration over the years is mainly associated with poor tolerability due to its gastrointestinal (GIT) side effects such as cinchonism, complex dosing regimen and bitter taste, all of which result in poor compliance. Hence, our research was aimed at redesigning quinine using nanotechnology and investigating an alternative route for its administration for the treatment of malaria. QHCl nanosuspension (QHCl-NS) for intranasal administration was prepared using lipid matrices made up of solidified reverse micellar solutions (SRMS) comprising Phospholipon® 90H and lipids (Softisan® 154 or Compritol®) in a 1:2 ratio, while Poloxamer® 188 (P188) and Tween® 80 (T80) were used as a stabilizer and a surfactant, respectively. The QHCl-NS formulated were in the nanosize range (68.60 ± 0.86 to 300.80 ± 10.11 nm), and highly stable during storage, though zeta potential was low (≤6.95 ± 0.416). QHCl-NS achieved above 80% *in vitro* drug release in 6 h. *Ex vivo* permeation studies revealed that formulating QHCl as NS resulted in a 5-fold and 56-fold increase in the flux and permeation coefficient, respectively, thereby enhancing permeation through pig nasal mucosa better than plain drug solutions. This implies that the rate of absorption as well as ease of drug permeation through porcine nasal mucosa was impressively enhanced by formulating QHCl as NS. Most importantly, reduction in parasitaemia in mice infected with *Plasmodium berghei* ANKA by QHCl-NS administered through the intranasal route (51.16%) was comparable to oral administration (52.12%). Therefore, redesigning QHCl as NS for intranasal administration has great potential to serve as a more tolerable option for the treatment of malaria in endemic areas.

Citation: Agbo, C.P.; Ugwuanyi, T.C.; Eze, O.C.; Onugwu, A.L.; Echezona, A.C.; Nwagwu, C.S.; Uzondu, S.W.; Ogbonna, J.D.; Ugorji, L.O.; Nnamani, P.O.; et al. Quinine: Redesigned and Rerouted. *Processes* **2023**, *11*, 1811. https://doi.org/10.3390/pr11061811

Academic Editors: Paolo Trucillo and Roberto Pisano

Received: 30 April 2023
Revised: 4 June 2023
Accepted: 7 June 2023
Published: 14 June 2023

Keywords: solidified reverse micellar solutions; nanostructured lipid carriers; quinine hydrochloride; intranasal route; severe malaria; cerebral malaria; parasitemia reduction

1. Introduction

The discovery of quinine in the 17th century and its use for malaria treatment was the first successful use of a chemical compound to treat an infectious disease. Unlike other antimalarials, the development of resistance to quinine (QHCl) has been slow, with the first reported case in 1910 [1], hence its use has continued to date. The decline in its administration over the years is mainly associated with poor tolerability due to its gastrointestinal side effects such as cinchonism (nausea, vomiting, dysphoria, tinnitus, and high-tone deafness). Adverse events such as hypoglycemia are also associated with quinine use, especially in pregnancy. Other drawbacks of quinine include its complex dosing regimen and bitter taste, all of which result in poor compliance [1].

Despite these shortcomings of quinine, its use has continued to date because of its defiance to resistance by malaria parasites. Intravenous (IV) quinine still finds use as a second-line treatment for severe malaria, after IV artesunate [2]. Quinine is considered safe for malaria treatment in all trimesters of pregnancy. Quinine in combination with doxycycline is effective against multidrug-resistant parasites [3]. Another important advantage of quinine compared to other antimalarials is its affordability; this is a major deciding factor in most endemic regions which also come under the low- or middle-income countries. For instance, in Nigeria, a complete dose of quinine for a seven-day course costs about $1.2, while a three-day treatment using artemether/lumefantrine (Coartem®) costs about $2.5.

Artemisinin-based combination therapy (ACT), which has become the mainstay for the treatment of uncomplicated malaria, is bedeviled with challenges including the development of resistance and high cost in resource-limited settings. Less than 50 years after its discovery in the 1970s, artemisinin resistance was first reported in 2009. Since then, a good number of reports have continued to surface of the malaria parasite's resistance to artemisinins [4]. There is therefore a great need to discover new, potent therapies for malaria or repurpose existing drugs [5].

Hence, our research was aimed at redesigning quinine using nanotechnology and investigating an alternative route for its administration for the treatment of malaria. To the best of our knowledge, no research investigating the intranasal administration of quinine for the treatment of malaria has been published. However, quinine nasal spray is being investigated for the prevention of infection by the SARS-CoV-2 virus [6]. In this study, a nanosuspension of quinine was formulated to suit intranasal administration.

The nasal cavity is highly vascularized with a relatively large surface area (96 m^2), making it an attractive route for drug administration [7]. Therefore, this route of drug administration can be exploited for drugs such as quinine, which are beset with numerous GIT side effects. The relatively reduced surface area of the nasal cavity compared to the GIT may reduce the rate of saturation of the systemic circulation with quinine, thereby preventing side effects such as cinchonism, which is dependent on the concentration of quinine in circulation [8]. The intranasal route also offers the advantage of ease of application and painless self-administration, just like the oral route. Unlike the oral route, drugs administered through this route can avoid first-pass metabolism, as well as achieve direct brain access through the olfactory region [9]. A previous study targeting intravenously administered quinine to the brain by means of conjugation to Transferrin, aimed at reducing the serum concentration, toxicity and improving efficacy in the treatment of cerebral malaria has been reported [10]. Other side effects that may be avoided by administering quinine through the nasal route include hypotension (which may occur when the drug is given too rapidly, e.g., through intravenous injection), venous thrombosis (this is usual with intravenous administration), pain and sterile abscesses at the site of injection (which happens when intramuscularly administered) [1]. Furthermore, delivery of quinine into

the brain through the nasal route in cerebral malaria patients would rapidly eradicate the parasite, averting the initiation of vascular occlusion and disseminated intravascular coagulation and neurological damage.

The rectal route is yet another route which may offer a slower administration of quinine, in addition to avoidance of GIT exposure; however, a negative cultural perception of the rectal route may limit its use [11].

Nanotechnology has been employed innovatively [12] for the revival of drugs and enhancement of their therapeutic potentials, in addition to the reduction of side-effect profiles [13], and enhancement of solubility of poorly water-soluble entities [14]. A good number of antiparasitic drugs such as halofantrine, primaquine, atovaquone as well as quinine [15] have been prepared as nanoformulations in order to improve drug solubility, enhance drug release, and achieve specific drug targeting. The designing of quinine as a nanocapsule was found to increase interaction between quinine and the erythrocyte, resulting in an increase in its *in vivo* efficacy in malaria-infected rats [15]. It is based on this premise that a nanosuspension of quinine was designed to suite intranasal administration.

In this study, the ability of the redesigned and rerouted quinine to treat malaria was investigated by formulating nanosuspension of quinine using different lipids. Characterization of NS was performed, after which QHCl-NS were administered intranasally to mice infected with *Plasmodium berghei* ANKA. The results obtained were compared with orally administered quinine and plain unprocessed quinine solution in water.

2. Materials and Methods

2.1. Materials

QHCl (purity $\geq$ 95%) was obtained from Sigma-Aldrich (England, UK). Softisan® 154 (S154) and Miglyol® 812 N (medium-chain triglycerides (MCT)) were gifts from IOI Oleo GmbH, (Witten, Germany). Compritol® 888 ATO (C888) (Glycerol dibehenate), Compritol® HD 5 ATO (CHD 5) (Behenoyl polyoxyl-8 glycerides), and Transcutol® HP (THP) (Diethylene glycol monoethyl ether) were also gifts from Gattefossé SAS (Saint-Priest Cedex, France). Free samples of Phospholipon® 90H (P90H) were obtained from Lipoid GmbH (Ludwigshafen, Germany). Stearic acid, Poloxamer® 188 (P188) and Tween® 80 (T80) were purchased from Sigma-Aldrich (England, UK). Ultrapure water was sourced from ELGA Purelab Ultra Genetic Water Purification System (UK). All other reagents were of analytical grade and purchased from standard commercial suppliers.

2.2. Methods

2.2.1. Determination of QHCl Solubility in Solid and Liquid Lipids

The solubility of QHCl in solid lipids (stearic acid, S154, CHD 5, and C888) as well as liquid lipids (Miglyol® 812 N and glyceryl monooleate) and the solvent (Transcutol® HP), were determined using a modified version of the shake-flask technique [16]. A 1:2 and 1:3 (*w*/*w*) ratio of the drug to lipid were prepared in each case and vortexed for 2 min. For the solid lipids, drugs were added to melted lipid (after 15 min heating at 10 °C above their melting temperatures). The solid and liquid lipids were selected for the formulation based on the transparency of the drug–lipid mixture [16].

2.2.2. Formulation of SRMS Lipid Matrices

The SRMS lipid matrices consisting of 1:2 (30:70) mixtures of P90H and either of the lipids: S154, or CHD 5, or C888, were prepared by fusion method [17]. Each of the lipids and P90H were weighed using an electronic balance (Mettler Toledo-X A204 Delta range), melted together on a hot plate (BioCote® Stuart hotplate stirrer) at 70 °C and stirred with the help of a magnetic bead at 200 rpm. The temperature was reduced to room temperature after melting, and mixing was completed to allow for solidification of lipid matrices. These were gently scraped out of the beakers and stored in air-tight glass bottles.

2.2.3. Preparation of QHCl-NS

QHCl-loaded NS were prepared by the combined ultrasonication technique, first with a cup-horn sonicator, and then a probe sonicator [9]. SRMS lipid matrix (3%) and MCT served as the solid and liquid lipids, respectively, while T80 (2, 3, or 5%) was the surfactant. P188 (1%) and sorbitol (5%) served as the stabilizer and cryoprotectant, respectively. First, melting of the solid lipid was done at 70 °C on a magnetic hot plate (BioCote® Stuart hotplate stirrer); subsequently, QHCl was dissolved in a mixture of THP and MCT and then added to the melted solid lipid matrix and mixed thoroughly at 300 rpm. An aqueous surfactant solution was added to the melted oil phase in drops with the help of a burette [18]. The aqueous surfactant solution contained T80, P188, and sorbitol and was heated to the same temperature as the lipid phase. The mixing of the two phases was carried out briefly on a magnetic stirrer at 70 °C before sonication was performed in a cup-horn sonicator for 30, 60, or 90 min at 100 amp at 43 °C. Additional sonication was achieved with a probe sonicator for 3 min at 70 °C. The same procedure was repeated for NS containing no drug (blanks), which served as placebos. All the NS were divided into two, one part was freeze-dried (Labconco FreeZone 6 Plus, Kansas City, MO, USA) at −80 °C and at a pressure of 0.01 mmHg, while the other portion was used for some characterizations and stability studies. The compositions of QHCl-NS and the cup-horn sonication times of different formulations are stated in Table 1.

Table 1. Quantities of materials used for the formulation of QHCl-NS.

QHCl-NS	Lipid Type	Concentration (%)							Cup-Horn Sonication Time (min)
		QHCl	Solid Lipid	MCT	THP	T80	P188	Sorbitol	
Q1	S154	1.5	3	1.5	1.5	3	1	5	30
Q3	S154	1.5	3	1.5	1.5	3	1	5	90
Q9	S154	1.5	3	1.5	1.5	2	1	5	60
Q10	S154	1.5	3	1.5	1.5	5	1	5	60
Q13	CHD 5	1.5	3	1.5	1.5	3	1	5	60
Q14	CHD 5	1.5	3	1.5	1.5	3	1	5	60
Q15	CHD 5	1.5	3	1.5	1.5	3	1	5	60
Q5	CHD 5	1.5	3	1.5	1.5	2	1	5	30
Q6	CHD 5	1.5	3	1.5	1.5	5	1	5	30
Q7	CHD 5	1.5	3	1.5	1.5	2	1	5	90
Q8	CHD 5	1.5	3	1.5	1.5	5	1	5	90
Q2	C888	1.5	3	1.5	1.5	3	1	5	30
Q4	C888	1.5	3	1.5	1.5	3	1	5	90
Q11	C888	1.5	3	1.5	1.5	2	1	5	60
Q12	C888	1.5	3	1.5	1.5	5	1	5	60

Key: QHCl = Quinine hydrochloride, **S154** = Softisan® 154, **C888** = Compritol® 888 ATO, **CHD 5** = Compritol® HD 5 ATO, **MCT** = Medium-Chain Triglyceride, **THP** = Transcutol® HP, **T80** = Tween® 80, **P188** = Poloxamer® 188.

2.2.4. Characterization of QHCl-NS

Determination of Particle Sizes, Polydispersity Indices, and Zeta (ζ) Potentials of NS

Particle size, polydispersity indices, and zeta potential determination was done using a nanosizer (Malvern-Zetasizer Nano series, Malvern Panalytical, Malvern, United Kingdom) immediately after formulation, as well as 30 and 90 days post formulation. Determination was carried out at 25 °C after dilution, and three replicates were obtained for each measurement. Data are presented as mean ± standard deviation (SD) [19].

Determination of the Morphology of QHCl-NS

(1) Transmission Electron Microscopy (TEM) of QHCl

A transmission electron microscope (JEOL JEM-1400 USA, Inc., Peabody, MA, USA) was used in the determination of the morphology of the QHCl-NS. Appropriate dilution of QHCl-NS (a 100 µL volume of each preparation diluted to 30 mL) using deionized water was done before placing NS on a 300-mesh carbon-coated copper grid (FC300Cu, Formvar/Carbon film on Copper). A drying time of two minutes was allowed to enable NS to adhere to the carbon substrate. Negative staining with 2% uranyl acetate and subsequent air-drying at room temperature for 1 min was carried out before observation was performed using TEM at 300 k magnification and voltage of 120 kV [9].

(2) Cryo-Scanning Electron Microscopy (cryo-SEM) and Field Emission SEM (FESEM) of NS

Morphological characterization was also done using cryo-SEM and field emission SEM. A drop of appropriately diluted QHCl-NS was placed on metal stubs and rapidly frozen with slush nitrogen until −210 °C and sublimated at −90 °C for 90 s. Coating was achieved with palladium under vacuum, and samples were fractured, transferred to the chamber, and examined using FESEM (Philips XL30 FEG ESEM). The observations were done at −150 °C [20], while micrographs were obtained at an accelerated voltage of 5 kV at a pressure of 0.6 mmHg [21]. Morphology of the dry samples (such as excipients, pure drug samples of quinine as well as freeze-dried NS) was carried out using normal FESEM. Samples were placed on double-sided tapes stuck to an aluminum stud. The samples were coated for three minutes with gold using a sputter coater (EMS 7620 Mini Sputter Coater/Glow Discharge System) with deposition control adjusted to 25 mA. Afterwards, the coated samples were loaded into FESEM (Philips XL30 FEG ESEM) and micrographs were obtained at an accelerated voltage of 15 kV, at a pressure of 0.6 mmHg [19].

Fourier Transform Infrared (FTIR) Spectroscopic Analysis

Fourier transform infrared spectroscopy (ATR-FTIR) of the freeze-dried QHCl-NS and excipients was performed on a PerkinElmer Spectrum fitted with a universal ATR sampling accessory and recorded in the range of 4000 to 650 cm^{-1} at ambient temperature. Evaluations were performed using a 16-scan-per-sample cycle and a fixed universal compression force of 80N. Subsequent analyses were carried out using spectrum software [17,22].

Thermal Analysis

Thermal analyses of freeze-dried samples of QHCl-NS, drug, physical mixtures of lipids and drug and other excipients were conducted using a differential scanning calorimeter (DSC) (TA Instruments, DSC-25, U.K.). Samples were weighed into aluminum pans, hermetically sealed, and determinations were performed at a heating rate of 10 °C/min over a temperature range of 10–200 °C under nitrogen purge at a flow rate of 80 cm^3/min. Data analyses, and the determination of melting points and enthalpies were done using TA Rheology Data Analysis software (TA Instruments Trios Version 4.1.33073, UK) [23].

Powder X-ray Diffractometry (XRD)

XRD patterns of drug, excipients, and QHCl-NS were obtained using a diffractometer (SIEMENS/BRUKER D5005, Munich, Germany). The samples were exposed to Cu-Kα radiation (40 kV, 35 mA), and measurements were carried out at room temperature. Scanning was carried out at 2θ from 5° to 90°, for 30 min (for excipients) or 1 h (for NS) [9].

Time-Dependent pH Stability Studies of NS

The pH of QHCl-NS as well as blanks were analysed in triplicate, and at room temperature on day 1, 30, and 90 using a pH meter (pHep® Hanna Instruments, Italy) [24].

Osmolality Determination

The osmolality determinations of NS were done using an Osmometer (Osmomat® 3000, Gonotec, Germany). A 100 µL quantity of each formulation was used, and the average of three determinations was obtained [25].

2.2.5. Solubility Analysis of QHCl in Simulated Nasal Fluid and Alcoholic Buffer

A concentration above the expected solubility level of QHCl (8%) was prepared in simulated nasal fluid (SNF) (8.77 g NaCl, 2.98 g KCl, and 0.59 g $CaCl_2$ per 1000 mL of demineralised water, pH of 6.4) [9]. Suspensions were kept in an incubator/shaker (Multitron Infors HT, Bottmingen, Switzerland) maintained at 37 ± 0.5 °C with continuous stirring at 100 rpm. After 24 h, samples were carefully withdrawn and filtered through 0.45 µm nylon syringe filters, diluted 1000 times, and analysed using HPLC [26].

2.2.6. In Vitro Release Studies of QHCl-NS

Release studies were conducted in SNF. Amounts of freeze-dried QHCl-NS containing 5 mg of the drugs were placed in polycarbonated dialysis membrane (length: 6 cm; pore size: 2.4 nm; molecular weight cut-off: 12, 000–14, 000 Da) which was previously soaked overnight in distilled water prior to the procedure, and immersed in 100 mL of release media [9,17]. The set-up was maintained at 37.0 ± 0.5 °C and stirred at 60 rpm for 24 h. At predetermined time intervals, a 1 mL portion of the dissolution media was withdrawn for HPLC analysis and replaced with 1 mL of fresh medium. The amount of drug released at each time point was calculated with reference to the relevant calibration plot. *In vitro* dissolutions of pure QHCl were also carried out following the same method. Each procedure was performed in triplicate. Kinetic evaluation of release profiles was done by fitting the data into zero-order, first-order, and Higuchi square root models [18]. The Korsmeyer–Peppas equation was also taken into consideration for determination of the release mechanism [27]. For the Korsmeyer–Peppas model, only the data points with less than 60% release were used for model fitting [28].

2.2.7. Ex Vivo Permeation Studies of QHCl-NS

Franz diffusion cells were used for the determination of the permeation efficacy of QHCl-loaded NS across porcine nasal mucosa from one selected formulation (Q9). Diffusion cells with a surface area of 6.6 cm^2 and volume of 10 mL were used. Appropriate volumes of deaerated SNF (pH 6.4) were placed in each of the Franz diffusion cells and allowed to equilibrate at 37.0 ± 0.5 °C for 15 min on a heated magnetic block. Fresh nasal pig tissue was obtained at the local slaughterhouse with prior permission from concerned authorities at the abattoir. Moreover, all animal experimental protocols were carried out in accordance with the guidelines of the Animal Ethics Committee of the University of Nigeria, Nsukka, and EU Directive 2010/63/EU for animal experiments. The nasal mucosa was detached from the septum, connective, and cartilaginous tissues and stored in phosphate-buffered saline (pH 6.4) during transportation. During each procedure, the nasal mucosa was individually placed on the Franz diffusion cells and clamped between the donor and receptor compartments, and sealed with Parafilm® to prevent loss of moisture during the 3 h period. Before sealing was done, amounts of Q9 NS containing 0.5 mg of QHCl were placed on the membrane surface on the donor compartment, and stirring was done at 600 rpm. A gel-loading pipette tip attached to a micropipette was used to withdraw 600 µL of the media from the receptor compartment at predetermined time intervals and replaced with the same volume of fresh SNF [18,29]. Permeations of pure unprocessed QHCl were also carried out to serve as the positive control. The results obtained were used to construct a permeation profile by plotting the amount of drug permeated per unit surface area (mg/cm^2) versus time (min). The steady-state flux (Jss, mg/cm^2 min) was calculated from the slope of the linear portion of the plot using linear regression analysis [9].

The drug apparent permeability coefficient (*Papp*) was calculated according to the equation:

$$Papp = \frac{dQ}{dt} \times \frac{1}{A.C_0.60} \quad (1)$$

where *Papp* is the apparent permeability coefficient (cm/s); dQ/dt is the cumulative amount of drug permeated vs. time per unit area (flux); A is the effective surface area (cm^2); and C_0 is the initial concentration ($\mu g/cm^3$).

2.2.8. In Vivo Pharmacodynamic Studies

The guidelines of the Animal Ethics Committee of the University of Nigeria, Nsukka, and EU Directive 2010/63/EU were observed while conducting the *in vivo* pharmacodynamic studies in mice. CBA/J mice, weighing 18–20 g, were made to develop malaria by intraperitoneal inoculation of 2×10^5 *Plasmodium berghei* ANKA-parasitized erythrocytes from a previously infected mouse [30,31]. Grouping into 5 sets of 6 was done on day seven (7) post infection, as shown in Table 2. Table 2 also shows the treatments administered, doses, as well as routes of administration.

Table 2. *In Vivo* studies design.

Formulation/API	Group	Treatment	Dosing	Route
QHCl	G1	Q9	20 mg/kg at 0 h, 10 mg/kg every 12 h for 4 days	IN
	G2	Plain QHCl solution		
	G3	Q9		Oral
Placebo	G4	Blank NS	20 mg/kg at 0 h, 10 mg/kg every 12 h for 4 days	IN
	G5			Oral

Key: **QHCl** = Quinine hydrochloride, **G1 to G4** = Groups of 6 mice; **Q9** = Q9 (QHCl-NS containing 1.5% *w*/*v* QHCl, 3% *w*/*v* S154, 2% *w*/*v* T80 and sonicated for 60 min); IN = Intranasal.

Mice receiving treatment intranasally were slightly anesthetized using ketamine at a dose of 75 mg/kg. To administer NS intranasally, each mouse was held using the left hand and restrained by anchoring the tail between the small finger and the palm [32,33], after which the mice were held in a supine position with the head elevated. Using the right hand, gel-loading tips attached to a micropipette were used to slowly introduce the right dose of each formulation through the external nares. Dose volumes were adjusted to $\leq$20 µL to avoid suffocation and death [34,35]. Mice were maintained in a standing position until they recovered from the effect of the anaesthesia. On day 13 post infection, each mouse was tail-bled, and a thin blood film was made on a microscope slide. The films were fixed with methanol, stained with gentian violet solution, and examined microscopically to monitor the parasitaemia level. The level of parasitaemia at day 1 post infection was used for comparison.

The percentage of parasitaemia in the blood was calculated using the expression:

$$\begin{gathered}\%\ \text{Reduction in Parasitaemia} = 100 - \\ \{\text{No. of parasitized RBC}/(\text{No. of parasitized RBC} + \text{No. of nonparasitized RBC})\} \\ \times 100\end{gathered} \quad (2)$$

Antimalarial activity of formulations and pure drug was determined by using the equation:

$$\text{Activity}(\%) = 100 - \left(\frac{\text{Mean parasitaemia in treated group}}{\text{Mean parasitaemia in control group}}\right) \times 100 \quad (3)$$

RBC (Red blood cell).

2.2.9. Histopathological Studies

After intranasal administration with Q9 NS, mice were sacrificed by cervical dislocation. Histopathological examination of samples collected from the nasal mucosa and lungs was conducted after the samples were fixed with 10% neutral-buffered formalin and dehydrated in graded concentrations of ethanol. Samples were subsequently cleared in xylene and embedded in paraffin wax. Exactly 5-µm-thick sections of the samples were cut and mounted on a glass slide, and later stained with hematoxylin and eosin (H & E). Micrographs of sections were captured using a Moticam Images Plus 2.0 digital camera (Motic China Group Ltd., Fujian, China) attached to a Leica binocular light microscope [36].

2.2.10. Data and Statistical Analysis

Results were expressed as mean ± standard deviation. For group comparisons, statistically significant differences were determined at $p < 0.05$ using one-way analysis of variance. Statistical analyses were done using GraphPad Prism version 8.2.0 (Prisma, Graphpad Software, La Jolla, CA, USA) [37].

3. Results and Discussion

3.1. Solubility of QHCl in Solid Lipids and Liquid Lipids

Since the solubility of any drug (especially hydrophilic drugs such as QHCl) is crucial in any lipid-based drug delivery system, the solubility of QHCl was analysed in selected solid and liquid lipids. Of all the solid lipids analysed, CHD 5 was a better solvent for QHCl, with stearic acid showing the least solubility (Table 3). Solubilization of QHCl in stearic acid was only possible after heating at 80 °C for up to 15 min. The Compritol® lipids (CHD 5 and C888) and S154 were selected for the preparation of NS, because QHCl was better solubilized in them and at lower temperatures. On the other hand, after the solubility test, QHCl was significantly dissolved in all the liquid lipids tested, with THP exhibiting the highest solubility. Hence, THP and Miglyol® 812 N were selected as the cosolvent and liquid lipid, respectively. Transcutol® HP, the highest purity grade of diethylene glycol monoethyl ether, has been known to exhibit good solubility for poorly soluble drugs such as risperidone [38] due to the presence of an ether and an alcohol functional groups in its molecule [39]. It is therefore used as cosolvent and surfactant. THP was also selected for use in this intranasal formulation due to its skin permeation enhancement property [40]. Despite its high solubility, it could not be used alone as the solvent, because it is toxic at high concentrations [41].

Table 3. Solubility of QHCl in solid and liquid lipids.

Solid Lipids	**Stearic Acid**	**Softisan® 154**	**Compritol® HD 5 ATO**	**Compritol® 888 ATO**
QHCl Solubility	+	++	+++	++
Liquid Lipids		Glyceryl monooleate	Transcutol® HP	
QHCl Solubility	+++	+++	++++	

Key: + = Sparingly soluble; ++ = Slightly soluble; +++ = Soluble; ++++ = Freely soluble, **QHCl** = Quinine hydrochloride.

3.2. Mean Particle Size and Particle Distribution Indices Analyses of QHCl-NS

Even though CHD 5 produced a higher solubility of QHCl, lipid matrices made with C888 and S154 were also used in the formulation of NS. In addition, three concentrations of surfactant and different sonication times were employed to determine the effect of varying these process parameters on average particle sizes and PDI of NS. All QHCl-NS had mean particles in the nanometer size range (68.60 ± 0.86 to 300.80 ± 10.11 nm) (Table 4; Figure 1).

Table 4. Particle size (24 h, 30 and 90 days), PDI and Zeta potential of QHCl-NS.

QHCl-NS	24 h			30 Days		90 Days	
	Particle Size (nm)	**PDI**	**Zeta Potential**	**Particle Size (nm)**	**PDI**	**Particle Size (nm)**	**PDI**
Q1	194.76 ± 4.495	0.441 ± 0.006	6.72 ± 0.259	199.27 ± 0.4225	0.433 ± 0.011	192.1 ± 2.371	0.427 ± 0.013
Q3	118.4 ± 0.7216	0.426 ± 0.017	3.24 ± 0.304	143.4 ± 0.6202	0.406 ± 0.2646	177.0 ± 3.704	0.237 ± 0.016
Q9	117.5 ± 1.53	0.282 ± 0.004	6.95 ± 0.416	112.2 ± 1.715	0.279 ± 0.004	113.7 ± 0.7550	0.279 ± 0.007
Q10	80.9 ± 1.57	0.465 ± 0.015	4.74 ± 0.371	68.15 ± 0.8786	0.456 ± 0.003	60.85 ± 0.5901	0.442 ± 0.013
Q13	92.9 ± 2.765	0.564 ± 0.032	4.81 ± 0.067	97.51 ± 0.767	0.431 ± 0.029	90.58 ± 0.747	0.315 ± 0.003
Q14	109.4 ± 0.814	0.599 ± 0.011	4.92 ± 0.096	115.2 ± 0.7092	0.443 ± 0.005	130.2 ± 0.4173	0.211 ± 0.011
Q15	120.5 ± 4.828	0.574 ± 0.027	4.28 ± 0.180	97.67 ± 1.640	0.425 ± 0.015	104.2 ± 0.7024	0.280 ± 0.003
Q5	83.52 ± 0.676	0.467 ± 0.008	6.19 ± 0.396	86.92 ± 0.999	0.319 ± 0.020	92.82 ± 0.5046	0.255 ± 0.010
Q6	150 ± 1.595	0.475 ± 0.007	5.36 ± 0.106	120.5 ± 0.808	0.371 ± 0.006	130.8 ± 0.625	0.268 ± 0.005
Q7	68.6 ± 0.861	0.491 ± 0.003	5.93 ± 0.18	79.9 ± 2.87	0.261 ± 0.010	87.31 ± 1.160	0.225 ± 0.005
Q8	90.36 ± 0.520	0.445 ± 0.003	4.36 ± 0.076	90.50 ± 2.859	0.307 ± 0.028	97.51 ± 0.197	0.307 ± 0.028
Q2	300.8 ± 10.11	0.603 ± 0.029	4.23 ± 0.294	206 ± 27.97	0.596 ± 0.146	186.9 ± 16.12	0.557 ± 0.073
Q4	121.5 ± 39.62	0.397 ± 0.132	2.31 ± 0.061	121.5 ± 39.62	0.397 ± 0.132	143.3 ± 1.739	0.441 ± 0.012
Q11	119.4 ± 0.945	0.511 ± 0.008	0.738 ± 0.138	109.1 ± 1.649	0.488 ± 0.006	113.2 ± 4.192	0.475 ± 0.017
Q12	118.6 ± 1.093	0.492 ± 0.022	2.16 ± 0.659	103.5 ± 1.580	0.434 ± 0.007	111.8 ± 4.925	0.318 ± 0.037

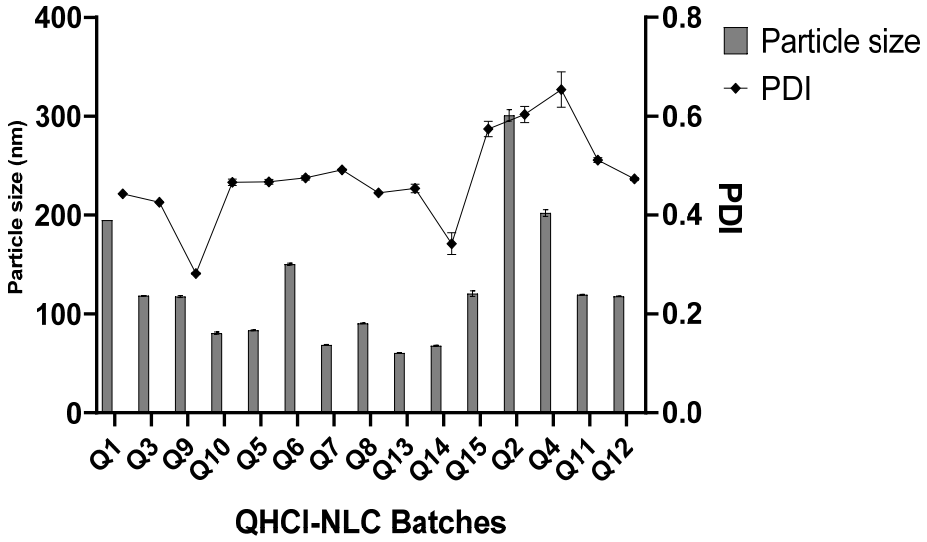

Figure 1. Particle size and PDI of QHCl-NS within 24 h.

In all the lipid matrices used, increasing sonication time from 30 to 90 min did better at reducing the particle size than increasing the surfactant concentration from 2 to 5%. In the case of QHCl-NS prepared with CHD 5 and C888, increasing the concentration of the surfactant resulted instead in an increase in particle size (compare Q5 and Q7, and Q6 and Q8, Figure 2). Hence, it can be concluded that it is not in all cases that increasing the concentration of the surfactant will result in a reduction in particle sizes [42]. Increasing the surfactant concentration may produce smaller particle sizes than increasing sonication time, especially when the concentration of the liquid lipid is high [9]. NS formulated with S154

produced more predictable results in terms of the particle sizes of QHCl-NS. Increasing sonication or the surfactant resulted in a reduction of particle sizes, even though increasing sonication time still yielded a smaller particle size better than using a higher concentration of surfactant (Q1 compared with Q3, and Q9 compared with 10; Table 4).

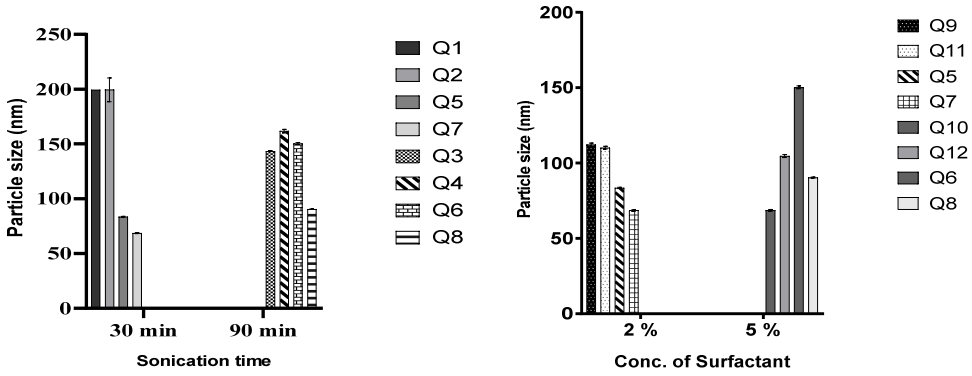

Figure 2. Effect of duration of sonication and concentration of T80 on particle size of QHCl-NS.

The differences observed in the particle sizes of the QHCl-NS made from the three lipid matrices can be attributed to their constituents and characteristics; S154 is hydrogenated palm oil made up of C14–C18 fatty acids and has a melting point of approximately 55 °C [43]; while C888 is docosanoic acid, monoester with glycerine, having a melting point of 69–74 °C. In addition to the constituents of C888, CHD 5 also contains poly(ethylene)glycol and melts at a lower temperature (56–63 °C) [44,45].

The PDIs of QHCl-NS formulations were in the range of 0.282 ± 0.004 to 0.603 ± 0.029 immediately after formulation, and the PDI of QHCl-NS prepared with C888 (Q2, Q4, and Q11) were all significantly higher ($p < 0.05$) than NS prepared with CHD 5, and especially S154 (Table 4). It was observed that PDI increased with a reduction in mean particle size. Thus, smaller particles had higher PDI than larger particles (compare Q9 with Q7 and Q10 in Table 4).

The nanosizes obtained may be beneficial to the usefulness of QHCl, since drugs in such sizes can access the brain through the olfactory region of the nasal cavity. It can also improve permeability through the nasal mucosa. Deductions made from the results on the influence of sonication of duration and concentration of surfactant show that these parameters significantly affect the final size of lipid nanoparticles. Therefore, preformulation studies to monitor average particle size while varying these parameters must be performed in order to determine the optimal conditions that would yield monodispersed, nano-sized lipid particles.

3.2.1. Stability Studies of QHCl-NS

The QHCl-NS formulated were very stable after 90 days. Only 6 formulations out of the 12 increased in size (negligibly) after 1 month. In some cases, a reduction in size and PDI was recorded (Table 4). This has been reported by other researchers [9,46,47] and is caused by a loss of solubilized water situated within the core of the nanoformulation. It may still be due to the ultrasonic energy used for size reduction, which is known to cause the collision of smaller oil droplets to form large ones [48,49], a phenomenon termed "sonication induced aggregate formation" [16,50]. Removal of the ultrasonic energy during storage may have led to a stable system resulting in a reduction in particle size and PDI. The high stability of the QHCl-NS formulation may be due to the surfactant (T80) and stabilizer use (P188) during formulation.

3.2.2. Surface Charge (Zeta (ζ) Potential) of NS

The low zeta potential values recorded for QHCl-NS (0.738 ± 0.138 to 6.720 ± 0.259 mV) are attributed to the use of non-ionic surfactants (T80 and P188) (Tables 4 and S1) [51].

The zeta potential of blank formulations was higher than that of the drug containing NS (Table S1). All QHCl-NS were positively charged within the first 24 h after preparation; however, some C888-containing formulations became slightly negatively charged after 30 and 90 days of storage. The low zeta potential did not cause an increase in sizes of nanoparticles in storage. This stability in sizes in storage may be due to the presence of P188, which is known to cause steric stabilization [52,53].

Three QHCl-NS formulations (Q7, Q9, and Q12) representing the three lipid matrices used (CHD 5, S154, and C888, respectively) were selected for further characterizations based on their acceptable particle sizes, PDI (highlighted on Table 4), and high stability during storage.

3.3. Time-Dependent pH Stability Studies and Osmolality of QHCl-NS

The pH of QHCl-NS formulations (5.03–5.55) were within the acceptable pH range for nasal formulations (pH of 4.5 to 6.5) [54], and remained stable for 90 days while being stored at 8 ± 2 °C (Figure 3). Osmolality of the formulations ranged from 422.3 ± 12.3 to 517.0 ± 21.7 mOsmol/kg (Table 5), which is within the range of most marketed nasal products (300–700 mOsmol/kg) [55]. Therefore, nasal irritation due to pH disparity or tonicity is unlikely to occur during administration.

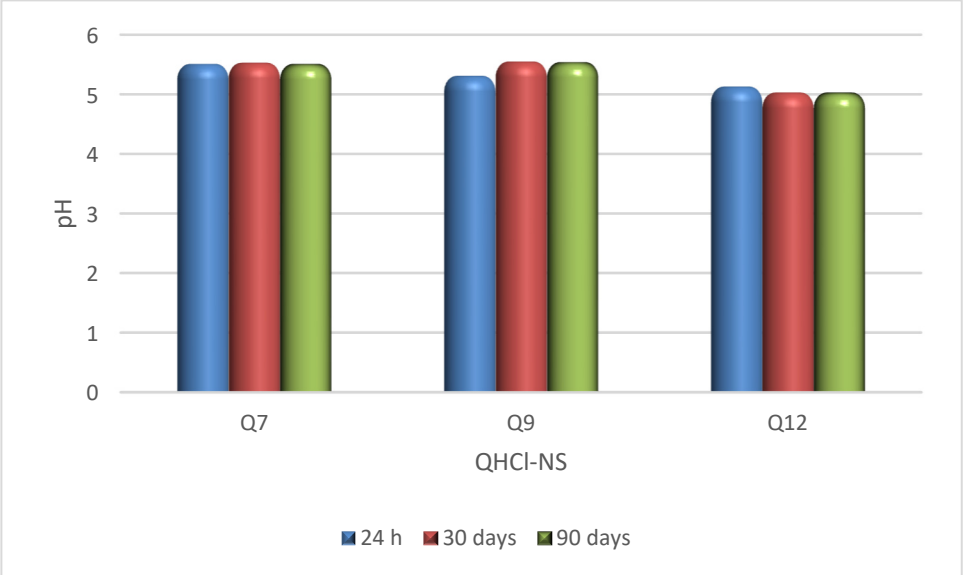

Figure 3. pH stability study of QHCl-NS.

Table 5. Osmolality, *ex vivo* permeation results and drug release mechanism and kinetics of QHCl-NS.

Batches	Osmolality (mOsmol/kg)	Flux (μg/cm^{2}min)	Permeation Coefficient (cm/s)	Zero Order	First Order	Higuchi	Korsmeyer–Peppas	
				r^2	r^2	r^2	r^2	*n*
Q7	422.3 ± 12.3	-	-	0.7807	0.9161	0.9939	0.9756	0.5055
Q9	492.7 ± 17.9	320.710	2.18×10^{-2}	0.7466	0.8885	0.9298	0.9993	0.8869
Q12	517.0 ± 21.7	-	-	0.8603	0.9611	0.9710	1	0.7730
Plain Solution of QHCl	-	56.973	3.87×10^{-4}	-	-	-	-	-

3.4. Morphology of QHCl-NS

The micrographs obtained from both TEM and SEM revealed round and oval-shaped particles (Figure 4A–D). During our experiments, we observed that cryo-SEM was a better method for visualizing NS compared to SEM (Figure 4C,D). Cryo-SEM was able to reveal more distinct particles (Figure 4D). The images obtained from SEM were clumped together, making visualization of individual particles difficult (Figure 4C). This difference may have been caused by lyophilization, since the samples used in SEM were lyophilized solid samples, while NS formulations in liquid form were used for cryo-SEM analysis. The micrographs of excipients and other NS formulations are presented in Figure S2.

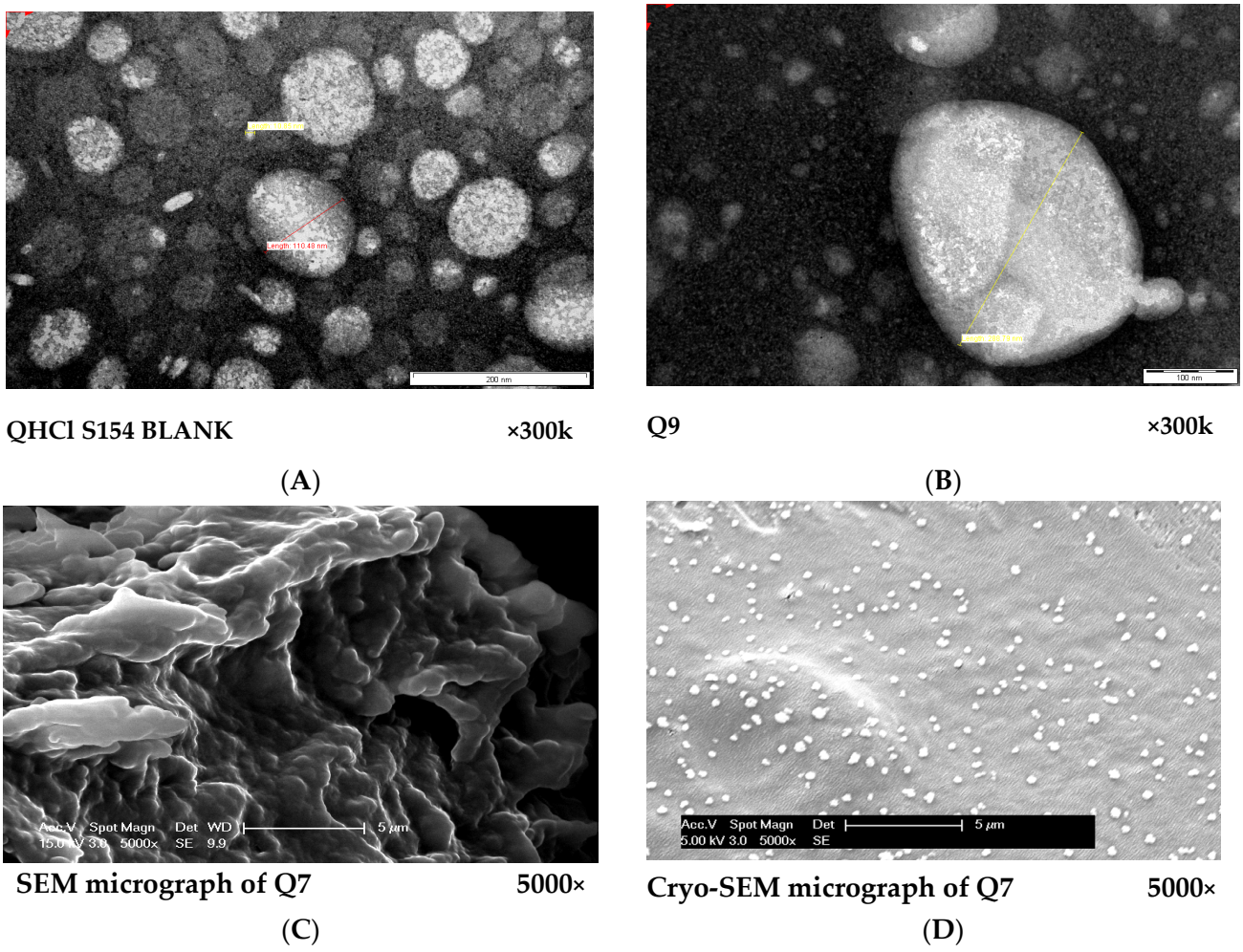

Figure 4. (**A**,**B**): TEM micrographs of S154 BLANK for QHCl-NS formulations (**A**) and Q9 (containing 1.5% *w*/*v* QHCl, 3% *w*/*v* S154, 2% *w*/*v* T80 and sonicated for 60 min). (**C**,**D**): Comparison between SEM (**C**) and cryo-SEM (**D**) micrographs of batch Q7 (containing 1.5% *w*/*v* QHCl, 3% *w*/*v* CHD 5, 2% *w*/*v* T80 and sonicated for 90 min).

3.5. FTIR Spectroscopic Analysis

A Fourier transform infrared spectrophotometer was used to determine possible interactions between the constituents of the lipid matrix (Softisan® 154, Compritol® HD 5 ATO and Compritol® 888 ATO, and Phospholipon® 90H) and between the lipid matrix and drug. The lipids (S154, CHD 5, and C888) were compatible with the P90H, as revealed in the FTIR spectra of the lipid matrices (Figure S2). The same principal peaks were evident in the FTIR spectra of the individual lipids and phospholipid as in the spectra of the lipid matrices. This suggests that the use of heat in the fusion of P90H and the lipids did not result in a chemical interaction.

In addition, FTIR results confirmed the lack of chemical interaction, and the compatibility of QHCl with the lipid matrices used as well as other excipients. Apart from the broadening and shortening of some principal peaks in the FTIR spectra of the selected formulations (Figure S2), no other difference was noticed. This difference may be attributed to hydrogen bond interactions as well as the presence of other excipients [27]. Hence, the designing of QHCl as a nanosuspension did not alter the chemistry of the drug, and it is expected not to lose its antimalaria activity.

3.6. Crystalline State of QHCl-NS

DSC analysis was conducted for unprocessed QHCl, excipients, and physical mixtures of the drug and lipids. All the solid lipids were crystalline in nature (sharp melting endothermic peaks at 57.68, 72.53, and 59.56 °C, enthalpies of 94.675, 116.25, and 117.83 J/g for pure S154, C888, and CHD5, respectively (Table S2)). P90H also showed an endothermic peak (122.30 °C). Fusion of the solid lipids with P90H during the formation of the SRMS caused reductions in melting points and enthalpies (Table S2). A complete disappearance of the melting peak due to P90H with the fusion of C888 and P90H implied that P90H was completely molecularly dispersed or amorphous in C888 (Figure S3) [56]. On the other hand, the inclusion of the liquid lipid (MCT) also caused further depression in the melting points of all solid lipid matrices, and so did the addition of Transcutol® HP (Table S2). The reduction of the melting points of solid lipids in the presence of liquid lipids and drugs has been previously reported by Garcia-Fuentes et al. [57] and Hu et al. [58]. Le-Jiao and coauthors [59] also reported a decrease in enthalpies of nanostructured lipid carriers with the addition of MCT. This is defined as a eutectic behaviour [56] and suggests a disordered lattice that can accommodate more drug molecules [9].

The melting point and enthalpy of unprocessed QHCl (117.29 °C) reduced when formulated as NS (57.11, 56.29, and 63.63 °C, for Q7, Q9, and Q12, respectively), suggesting amorphization (Figure 5). However, this was further investigated using X-ray diffractometry, because it may be erroneous to conclude on the crystal nature of a drug using DSC when it is available in low concentrations (less than 10%) [9].

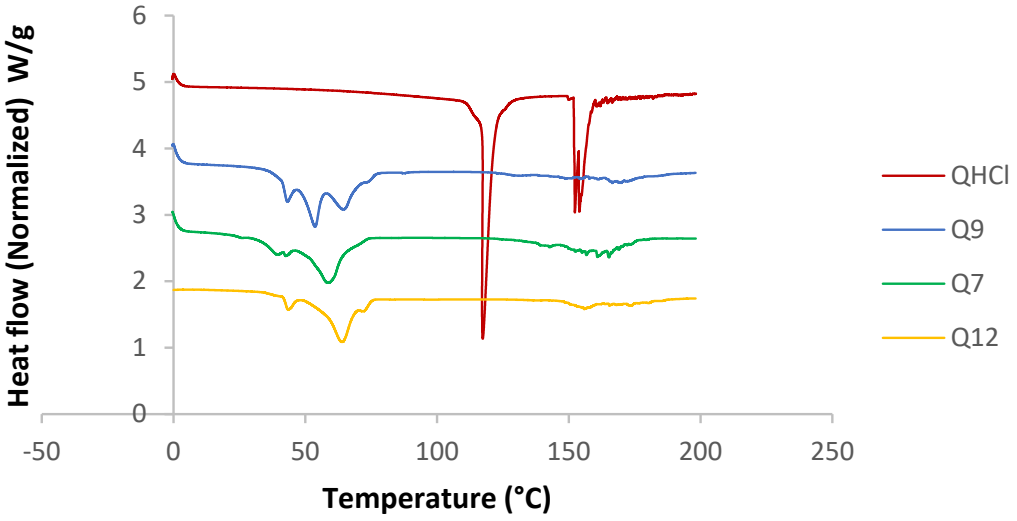

Figure 5. DSC thermogram of selected batches from QHCl-NS.

3.7. Powder X-ray Diffractometry of NS

X-ray diffractograms of QHCl-NS confirmed a reduction in crystallinity, since there were disappearances of some peaks in the diffractogram of the NS, unlike in the unprocessed drug (Figure 6A–D). For instance, some peaks in unprocessed QHCl at 2θ of 10° to 20° (Figure 6A) were not seen in Q7 (Figure 6B), while peaks at 2θ of 13.4° and 24.0° in pure QHCl were lost in Q9 (Figure 6C). Also, so many sharp peaks were not visible in Q12 (Figure 6D) compared to the pure quinine hydrochloride. For example, sharp distinct

peaks at 2θ of 9.2°, 14.6°, 17.9°, and 23.9° to 48.9° in pure quinine sample were not detected in Q12 (Figure 6D). Amorphous halos were also very visible on the XRD patterns of the NS; an indication of the presence of some amorphous form of the drug. It can therefore be concluded that QHCl were in microcrystalline or semi-crystalline form in the NS [60,61].

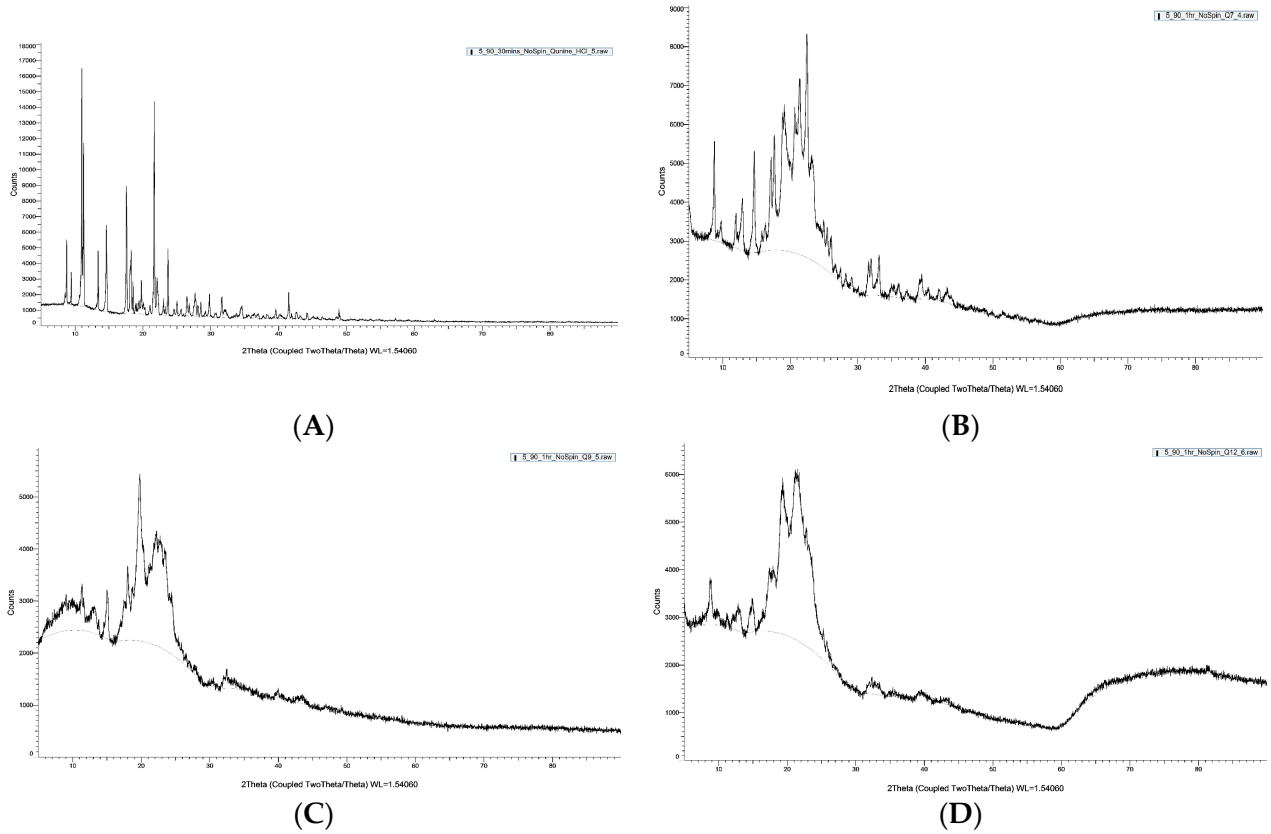

Figure 6. XRD pattern of pure sample of (**A**) QHCl, (**B**) Q7, (**C**) Q9, (**D**) Q12.

3.8. In Vitro Release Studies of QHCl-NS

3.8.1. *In Vitro* Release of QHCl-NS

In Vitro drug release was conducted in SNF in order to mimic the nasal environment. The solubility of QHCl in SNF was determined to be 26.49 mg/mL. The sink condition was maintained throughout the procedure by using a volume that will accommodate a solubilized drug without saturation occurring, as well as by replenishing with fresh media after each withdrawal of samples for analyses. Neither the concentration of surfactant nor particle size significantly influenced drug release among QHCl-loaded formulations (Figure 7). This may have been due to the high solubility of QHCl in the release media (26.49 mg/mL). Although pure unprocessed QHCl released slightly more drug than all the selected QHCl formulations (Q7, Q9, Q12), after the 6th hour, all formulations released above 80% of their drug content, with Q9 (formulated with S154) NS showing the fastest rate of release. The faster rate of release of pure unprocessed API compared to drugs in nanoformulations has been reported by other researchers [28] and may be attributed to time required for the release media to bypass the lipid carrier system wherein the drug is encapsulated or dispersed.

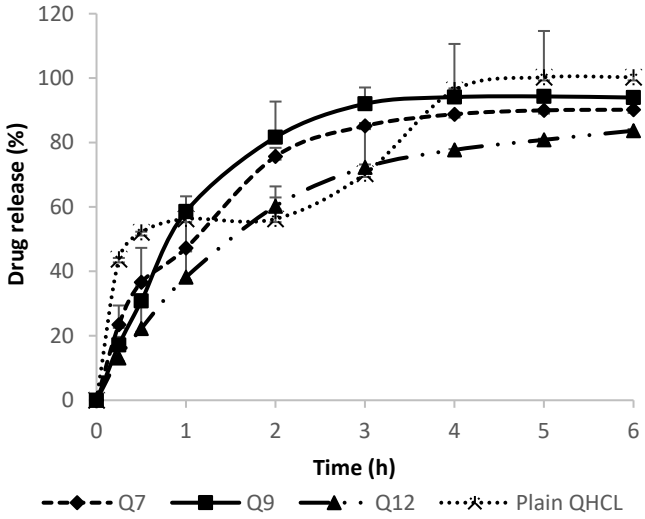

Figure 7. *In Vitro* release of QHCl from NS in simulated nasal fluid.

3.8.2. Evaluation of Drug Release Mechanism and Kinetics of QHCl-NS

Zero-order, first-order and Higuchi mathematical models were used to evaluate the kinetics of drug release from NS. The model that gave the highest correlation coefficient value was considered the best fit for the release data being analysed [27,62]. Drug release from all QHCl-NS followed Higuchi release kinetics (Table 5). The mechanism of drug release was determined using the Korsmeyer–Peppas model (Table 5). The "*n*" value for Q7 was 0.5055, indicating a Fickian diffusion-controlled mechanism. Diffusion of quinine from Q9 and Q12 was by anomalous diffusion, implying that the release of quinine from these NS formulations was by both diffusion and erosion of the lipid matrix, since the diffusional release exponent was greater than 0.5 but less than 1 (Table 5).

3.9. Ex Vivo Permeation Analysis of QHC1-NS

The *ex vivo* permeation analysis and the *in vivo* antimalarial study were conducted using only Q9, because this formulation exhibited a higher *in vitro* release than the other selected formulations (Q7 and Q12). The results obtained were compared with the unprocessed QHCl to determine the effect of formulating quinine as NS. The flux and permeation coefficient of Q9 (320.71 $\mu g/cm^2 min$ and 2.18 $\times$ 10^{-2} cm/s, respectively) were significantly ($p < 0.05$) higher than that of the unprocessed pure sample of QHCl (56.97 $\mu g/cm^2 min$ and 3.87 $\times$ 10^{-4} cm/s, respectively) (Table 5). A 5-fold and 56-fold increase in the flux and permeation coefficient, respectively, were observed. This implies that the rate of absorption as well as ease of drug permeation through porcine nasal mucosa was impressively enhanced by formulating QHCl as NS. A similar outcome has been earlier reported for artesunate NLC and gentamicin lipid-based microsuspension [9,25]. The lipophilicity of NS improved the permeation of QHCl, a hydrophilic drug, through excised porcine nasal mucosa. This also implies that the reformulation of QHCl can improve its permeation through lipid bilayers.

3.10. In Vivo Antimalarial Studies of QHCl-NS

Antimalarial investigation showed that there was a significant ($p < 0.05$) reduction of parasitaemia achieved with both intranasal and oral administration of QHCl-NS compared with the placebo. The reductions in parasitaemia caused by Q9 administered through the intranasal and oral routes were 51.16% and 52.12%, respectively (Figure 8). Interestingly, reductions in parasitaemia observed in both routes of administration were similar and not significantly different, though that of the oral route was higher. This is an indication that malaria treatment with quinine through the intranasal route is a possibility. The activity of the drug when given through the nasal route (56.26%) was higher than when administered

through the oral route (54.22%) (Figure 9). The administration of unprocessed quinine solution exhibited a significantly ($p < 0.05$) higher reduction in parasitaemia and activity. This varies from the results obtained in the *ex vivo* permeation studies. However, for the intranasal administration, an NS formulation of quinine will still be preferrable, because such a formulation being mucoadhesive will be better retained in the nasal region [63]. A plain solution of the drug may easily be cleared in the nasal cavity, as well as run off to the oral region of the mouth or throat, causing the patient to experience an unpleasant taste.

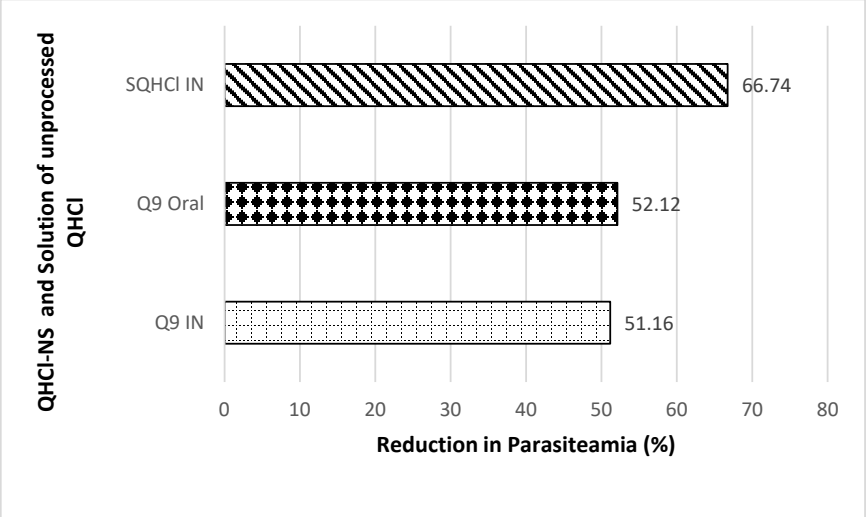

Figure 8. Percentage reduction in parasitaemia after IN and oral treatment with Q9 NS formulation and plain solution of QHCl (SQHCl).

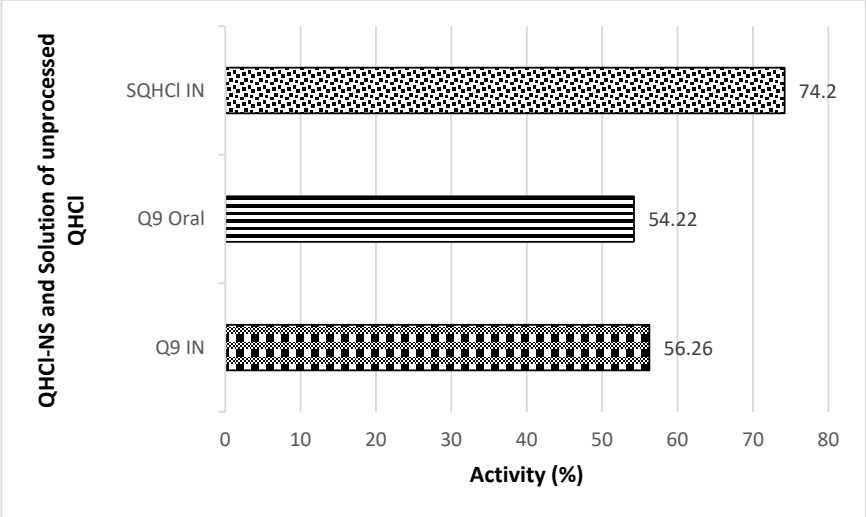

Figure 9. *In Vivo* antimalarial activity after IN and oral treatment with Q9 NS formulation and plain solution of QHCl (SQHCl).

3.11. Histopathological Studies

The histopathological analysis of the lungs and the nasal mucosa showed a clear difference between the treated and the untreated groups. While there was evidence of inflammation and congestion of red blood cells in the lungs and nasal mucosa of the mice in the untreated group (Figures 10A and 11A), none was observed in the lungs and nasal mucosa of mice treated intranasally with Q9 (Figures 10B and 11B,C). The observed congestion of pulmonary vessels in the mice treated intranasally with placebo is indicative of severe malaria [64]. No sign of injury was seen in the group treated with Q9 through the

intranasal route (Figures 10B and 11B,C). However, the pseudostratified columnar ciliated epithelium and nonciliated goblet cells covered by thin mucus membrane were intact in both groups and undamaged by intranasal administration of formulation and placebo. This implies that intranasal administration of NS formulation of QHCl for the treatment of malaria caused no damage to the nasal mucosa.

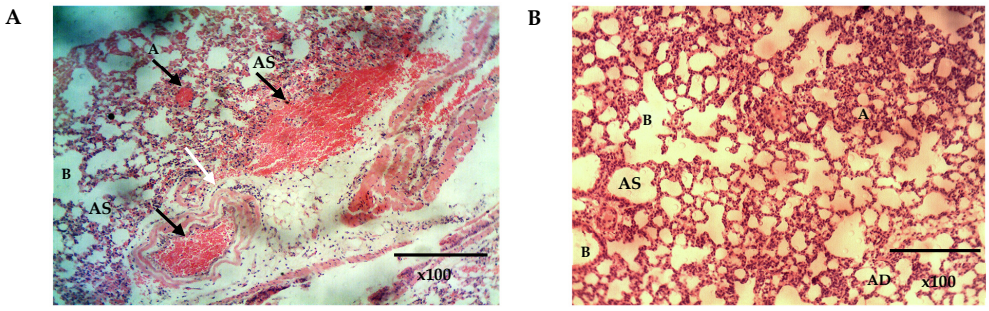

Figure 10. The histomicrograph of the lungs of mice treated with placebo (**A**) and Q9 (**B**) H & E ×100, showing normal respiratory epithelium of the smaller bronchioles (**B**) (arrows: ciliated simple columnar epithelium). Note also the normal Alveolar duct (AD), Alveolar sac (AS), and Alveoli (**A**) in A and B, and the sequestration of parasitized red blood cells (black arrows) and congested pulmonary vessels (white arrows) in (**A**). (For interpretation of the references to colour in this figure legend, the reader is referred to the web version of this article).

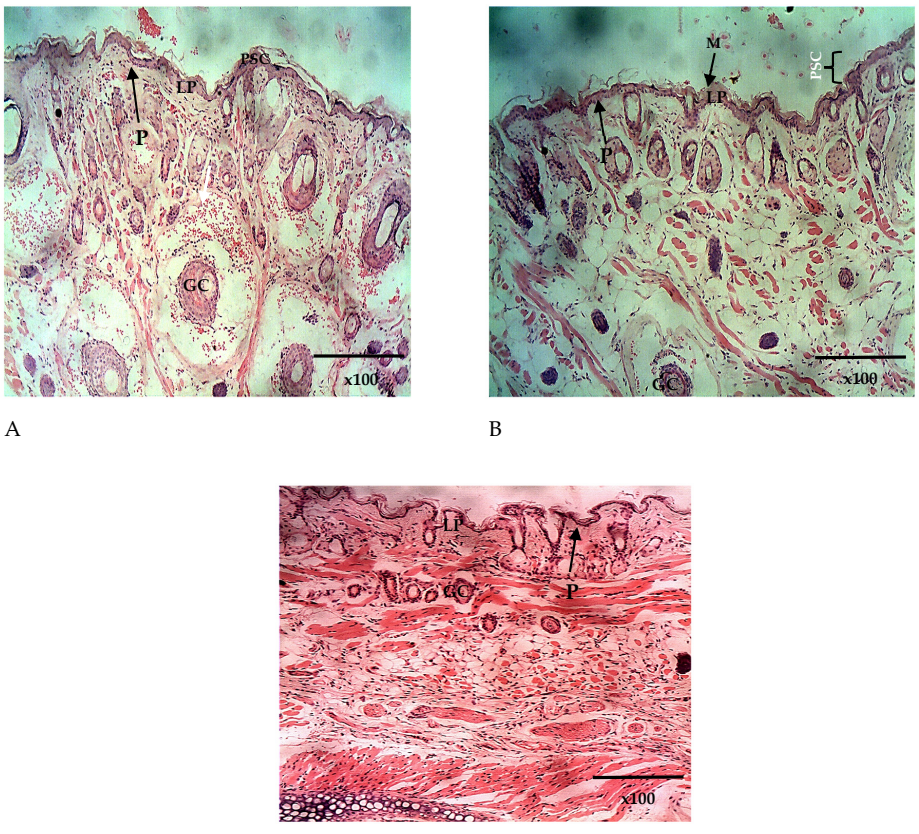

Figure 11. The histomicrograph of the nasal epithelium of mice treated intranasally with placebo (**A**) and Q9 (**B**,**C**) H & E ×100, showing the nasal epithelium (epidermis; P) composed of pseudostratified columnar ciliated epithelium (PSC) and covered by mucus membrane ((**C**); MM). Note also the goblet cells (GC) and the lamina propria (LP). H & E ×100 (**A**–**C**). The sequestration of parasitized red blood cells (white arrows).

4. Conclusions

Intranasal administration of QHCl-NS successfully treated malaria in mice infected with *Plasmodium berghei* ANKA, and can therefore serve as an alternative to other routes of administration of QHCl for the treatment of malaria. It can be beneficial in preventing the GIT-associated side effects caused by QHCl and can be helpful to patients (especially pregnant woman) who may be having the side effect of vomiting due to morning sickness and malaria. The relatively reduced surface area of the nasal cavity compared to the GIT may reduce the rate of saturation of the systemic circulation with quinine, thereby preventing cinchonism, which is dependent on the concentration of quinine in circulation. The intranasal route also offers the advantage of ease of application, painless self-administration, avoidance of first-pass metabolism, and direct access to the brain in the case of cerebral malaria. The results of the *ex vivo* studies revealed the potential of the nanosuspension of QHCl improving permeation through the nasal mucosa. Its bioadhesive nature compared to unprocessed QHCl solution will increase the residence time of the drug in the nasal cavity and retard flow of the bitter-tasting drug to the oral cavity.

Further studies to compare parenteral administration of QHCl to intranasal administration, as well as quantification of the amount of drug in the brain relative to systemic circulation after intranasal administration, will be conducted.

Supplementary Materials: The following supporting information can be downloaded at: https://www.mdpi.com/article/10.3390/pr11061811/s1: Table S1: zeta potentials of blank-NS formulations; Figure S1: SEM micrographs of drug and some excipients; Figure S2: FTIR Spectra of Excipients and QHCl-NS formulation; Table S2: DSC analysis results of plain drugs, and lipids and lipid matrices; Figure S3: DSC thermogram of lipid matrix made with C888 and P90H.

Author Contributions: Conceptualization, C.P.A., P.A.A., J.N.R.-O., C.M. and A.A.A.; data curation, T.C.U.; formal analysis, C.P.A., J.N.R.-O., C.M. and A.A.A.; funding acquisition, P.A.A., C.M., A.A.A., M.A.M. and K.C.O.; investigation, T.C.U. and K.C.O.; methodology, C.P.A., T.C.U., J.D.O., L.O.U., P.O.N., C.M., A.A.A. and K.C.O.; project administration, C.P.A., C.M. and M.A.M.; resources, K.C.O.; validation, J.N.R.-O. and J.O.O.; visualization, O.C.E.; writing—original draft, C.P.A. and T.C.U.; writing—review and editing, C.P.A., O.C.E., A.L.O., A.C.E., C.S.N., S.W.U., J.D.O., P.O.N., J.N.R.-O. and C.M. All authors have read and agreed to the published version of the manuscript.

Funding: The conducting of the research work was funded by the Commonwealth Scholarshipa Commission in the United Kingdom and 2021 African–German Network of Excellence in Science-Programme Advocating Women in Science (AGNES-PAWS) Grant for Junior Researchers, supported by the Federal Ministry of Education and Research (BMBF) and the Alexander von Humboldt Foundation (AvH). The funders provided financial support but did not influence the study design, analysis, and interpretation of data generated.

Institutional Review Board Statement: The study was conducted in accordance with the National Code of Conduct for Animal Research Ethics (NCARE). The animal study protocol was approved by the Animal Research Ethics Committee of the University of Nigeria, Nsukka (7 February 2019).

Informed Consent Statement: Not applicable.

Data Availability Statement: Not applicable.

Acknowledgments: We wish to thank the management of the University of Nigeria, Nsukka, and the University of Birmingham, where this research was conducted. Our appreciation also goes to Lipoid GmbH and IOI Oleo GmbH for the gift of Phospholipon® 90H, Softisan® 154, Compritol® 888 ATO, Compritol® HD5 ATO, Transcutol® HP, Transcutol® P, and Miglyol® 812 N. Our sincere appreciation also goes to Offor Ejike, Nwabueze Harrison, Ubachukwu Ugochukwu, Ugwu Chinedu, Fredrick Ugwuoke, Gábor Drávavölgyi, Hanouf Bafhaid, Ali Al Amri, Sarah Lastakchi, Justyna Hofmanová, and Sandya Rajesh for assisting in the laboratory procedures and the animal studies.

Conflicts of Interest: The authors declare no conflict of interest. The funders had no role in the design of the study; in the collection, analyses, or interpretation of data; in the writing of the manuscript, or in the decision to publish the results.

References

1. Achan, J.; Talisuna, A.O.; Erhart, A.; Yeka, A.; Tibenderana, J.K.; Baliraine, F.N.; Rosenthal, P.J.; Alessandro, U.D. Quinine, an Old Anti-Malarial Drug in a Modern World: Role in the Treatment of Malaria. *Malar. J.* **2011**, *10*, 144. [CrossRef] [PubMed]
2. World Health Organization. *Guideline for the Treatment of Malaria*, 3rd ed.; World Health Organization: Geneva, Switzerland, 2015. [CrossRef]
3. Fairhurst, R.M.; Wellems, T.E. Malaria (Plasmodium Species). In *Mandell Douglas, and Bennett's Principles and Practice of Infectious Diseases*; Elsevier: Amsterdam, The Netherlands, 2019; pp. 3070–3090.
4. Fairhurst, R.M.; Dondrop, A.M. Artemisinin-Resistant Plasmodium Falciparum Malaria. *Microbiol. Spectr.* **2016**, *4*, 4-3. [CrossRef] [PubMed]
5. Uzondu, S.; Echezona, A.; Nwagwu, C.; Onugwu, A.; Ugorji, L.; Agbo, C.; Kenechukwu, F.; Ogbonna, J.; Akpa, P.; Nnamani, P.; et al. *Combating Antimalarial Drug Resistance: Recent Advances and Future Perspectives*; IntechOpen: London, UK, 2022; pp. 1–16. [CrossRef]
6. U.S. National Library of Medicine. GLS-1200 Topical Nasal Spray to Prevent SARS-CoV-2 Infection (COVID-19). NCT04408183. Available online: https://clinicaltrials.gov/ct2/show/NCT04408183 (accessed on 31 August 2022).
7. Gizurarson, S. Anatomical and Histological Factors Affecting Intranasal Drug and Vaccine Delivery. *Curr. Drug Deliv.* **2012**, *9*, 566–582. [CrossRef] [PubMed]
8. Quinine. In *Meyler's Side Effects of Drugs*; Aronson, J.K. (Ed.) Elsevier: Oxford, UK, 2016; pp. 27–35. [CrossRef]
9. Agbo, C.P.; Ugwuanyi, T.C.; Ugwuoke, W.I.; McConville, C.; Attama, A.A.; Ofokansi, K.C. Intranasal Artesunate-Loaded Nanostructured Lipid Carriers: A Convenient Alternative to Parenteral Formulations for the Treatment of Severe and Cerebral Malaria. *J. Control. Release* **2021**, *334*, 224–236. [CrossRef]
10. Gupta, Y.; Jain, A.; Jain, S.K. Transferrin-conjugated Solid Lipid Nanoparticles for Enhanced Delivery of Quinine Dihydrochloride to the Brain. *J. Pharm. Pharmacol.* **2007**, *59*, 935–940. [CrossRef]
11. Marijon, A.; Bonnot, G.; Fourier, A.; Bringer, C.; Lavoignat, A.; Gagnieu, M.-C.; Bienvenu, A.-L.; Picot, S. Efficacy of Intranasal Administration of Artesunate in Experimental Cerebral Malaria. *Malar. J.* **2014**, *13*, 501. [CrossRef]
12. Torrino, E.; De Marco, I.; Reverchon, E. Organic Nanoparticles Recovery in Supercritical Antisolvent Precipitation. *J. Supercrit. Fluids* **2010**, *55*, 300–306. [CrossRef]
13. Mumuni, M.A.; Frankline, K.C.; Ugwu, C.E.; Musiliu, A.O.; Agboke, A.A.; Agbo, P.; Ossai, E.C.; Ofomata, A.C.; Youngson, D.C.; Omeje, C.E.; et al. Development and Evaluation of Artemether-Loaded Microspheres Delivery System for Oral Application in Malaria Treatment. *Trop. J. Nat. Prod. Res.* **2021**, *5*, 2030–2036.
14. Wang, C.; Yan, T.; Yan, T.; Wang, Z. Fabrication of Hesperetin/Hydroxypropyl-B-Cyclodextrin Complex Nanoparticles for Enhancement of Bioactivity Using Supercritical Antisolvent Technology. *J. Mol. Struct.* **2023**, *1279*, 134947. [CrossRef]
15. Haas, S.E.; Bettoni, C.C.; de Oliveira, L.K.; Guterres, S.S.; Costa, T.D. Nanoencapsulation Increases Quinine Antimalarial Efficacy against *Plasmodium berghei In Vivo*. *Int. J. Antimicrob. Agents* **2009**, *34*, 156–161. [CrossRef]
16. Shah, B.; Khunt, D.; Bhatt, H.; Misra, M.; Padh, H. Application of Quality by Design Approach for Intranasal Delivery of Rivastigmine Loaded Solid Lipid Nanoparticles: Effect on Formulation and Characterization Parameters. *Eur. J. Pharm. Sci.* **2015**, *78*, 54–66. [CrossRef] [PubMed]
17. Agbo, C.; Umeyor, C.; Kenechukwu, F.; Ogbonna, J.; Chime, S.; Lovelyn, C.; Agubata, O.; Ofokansi, K.; Attama, A. Formulation Design, *in vitro* Characterizations and Anti-Malarial Investigations of Artemether and Lumefantrine-Entrapped Solid Lipid Microparticles. *Drug Dev. Ind. Pharm.* **2016**, *42*, 1708–1721. [CrossRef] [PubMed]
18. Jain, K.; Sood, S.; Gowthamarajan, K. Optimization of Artemether-Loaded NLC for Intranasal Delivery Using Central Composite Design. *Drug Deliv.* **2015**, *22*, 940–954. [CrossRef] [PubMed]
19. Gaba, B.; Fazil, M.; Khan, S.; Ali, A.; Baboota, S.; Ali, J. Nanostructured Lipid Carrier System for Topical Delivery of Terbinafine Hydrochloride. *Bull. Fac. Pharm. Cairo Univ.* **2015**, *53*, 147–159. [CrossRef]
20. Tichota, D.M.; Silva, A.C. Design, Characterization, and Clinical Evaluation of Argan Oil Nanostructured Lipid Carriers to Improve Skin Hydration. *Int. J. Nanomed.* **2014**, *20*, 3855–3864.
21. Pretorius, E. Influence of Acceleration Voltage on Scanning Electron Microscopy of Human Blood Platelets. *Microsc. Res. Technol.* **2010**, *73*, 225–228. [CrossRef]
22. Jiang, Y.; Meng, X.; Wu, Z.; Qi, X. Modified Chitosan Thermosensitive Hydrogel Enables Sustained and Efficient Anti-Tumor Therapy via Intratumoral Injection. *Carbohydr. Polym.* **2016**, *144*, 245–253. [CrossRef]
23. Mallappa, P.; Prabirkumar, S.; Panchakshari, A. Taste Masked Quinine Sulphate Loaded Solid Lipid Nanoparticles for Flexible Pediatric Dosing. *Indian J. Pharm. Educ. Res.* **2014**, *48*, 93–99. [CrossRef]
24. Momoh, M.A.; Franklin, K.C.; Agbo, C.P.; Ugwu, C.E.; Adedokun, M.O.; Anthony, O.C.; Chidozie, O.E.; Okorie, A.N. Microemulsion-Based Approach for Oral Delivery of Insulin: Formulation Design and Characterization. *Heliyon* **2020**, *6*, e03650. [CrossRef]
25. Onugwu, A.L.; Agbo, C.P.; Nwagwu, C.S.; Uzondu, E.; Echezona, A.C.; Dike, J.; Ogbonna, N.; Akpa, P.A.; Momoh, M.A.; Nnamani, P.O.; et al. Development of Lipid-Based Microsuspensions for Improved Ophthalmic Delivery of Gentamicin Sulphate. *Ther. Deliv.* **2021**, *12*, 671–683. [CrossRef]
26. FDA. *Dissolution Methods Database*; FDA: Washington, DC, USA, 2019.

27. Ümİt, G.; Melİke, Ü.; Gülgün, Y.; Ecem Fatma, K.; Aydoğmuş, Z. Formulation and Characterization of Solid Lipid Nanoparticles, Nanostructured Lipid Carriers and Nanoemulsion of Lornoxicam for Transdermal Delivery. *Acta Pharm.* **2015**, *65*, 771–791. [CrossRef]
28. Weng, J.; Tong, H.H.Y.; Chow, S.F. *In vitro* Release Study of the Polymeric Drug Nanoparticles: Development and Validation of a Novel Method. *Pharmaceutics* **2020**, *12*, 732. [CrossRef]
29. Ng, S.F.; Rouse, J.; Sanderson, D.; Eccleston, G. A Comparative Study of Transmembrane Diffusion and Permeation of Ibuprofen across Synthetic Membranes Using Franz Diffusion Cells. *Pharmaceutics* **2010**, *2*, 209–223. [CrossRef]
30. Clemmer, L.; Martins, Y.C.; Zanini, G.M.; Frangos, J.A.; Carvalho, L.J.M. Artemether and Artesunate Show the Highest Efficacies in Rescuing Mice with Late-Stage Cerebral Malaria and Rapidly Decrease Leukocyte Accumulation in the Brain. *Antimicrob. Agents Chemother.* **2011**, *55*, 1383–1390. [CrossRef] [PubMed]
31. Craig, A.G.; Grau, G.E.; Janse, C.; Kazura, J.W.; Milner, D.; Barnwell, J.W.; Turner, G.; Langhorne, J.; on behalf of the participants of the Hinxton Retreat meeting on "Animal Models for Research on Severe Malaria". The Role of Animal Models for Research on Severe Malaria. *PLoS Pathog.* **2012**, *8*, e1002401. [CrossRef]
32. Shimizu, S. Routes of Administration. In *The Laboratory Mouse (Handbook of Experimental Animals)—USP*; Elsevier: Tsukuba, Japan, 2004; pp. 527–541.
33. Simmons, M.L.; Brick, J.O. *The Laboratory Mouse*; Hollaender, A., Ed.; Prentice-Hall Inc.: Englewood Cliffs, NJ, USA, 1970.
34. Shen, X.; Lagergård, T.; Yang, Y.; Lindblad, M.; Fredriksson, M.; Holmgren, J.A.N.; Mmun, I.N.I. Group B Streptococcus Capsular Polysaccharide-Cholera Toxin B Subunit Conjugate Vaccines Prepared by Different Methods for Intranasal Immunization. *Infect. Immun.* **2001**, *69*, 297–306. [CrossRef]
35. Shen, X.; Lagergård, T.; Yang, Y.; Lindblad, M.; Fredriksson, M.; Holmgren, J.A.N. Systemic and Mucosal Immune Responses in Mice after Mucosal Immunization with Group B Streptococcus Type III Capsular Polysaccharide-Cholera Toxin B Subunit Conjugate Vaccine. *Infect. Immun.* **2000**, *68*, 5749–5755. [CrossRef] [PubMed]
36. Ashoori, Y.; Mohkam, M.; Heidari, R.; Abootalebi, S.N.; Mousavi, S.M.; Hashemi, S.A.; Golkar, N.; Gholami, A. Development and *In vivo* Characterization of Probiotic Lysate- Treated Chitosan Nanogel as a Novel Biocompatible Formulation for Wound Healing. *Biomed Res. Int.* **2020**, *2020*, 8868618. [CrossRef]
37. Gratieri, T.; Martins, G.; Melani, E.; Hugo, V.; Freitas, O.; De Fonseca, R.; Lopez, V. A Poloxamer/Chitosan in Situ Forming Gel with Prolonged Retention Time for Ocular Delivery. *Eur. J. Pharm. Biopharm.* **2010**, *75*, 186–193. [CrossRef] [PubMed]
38. Khames, A. Investigation of the Effect of Solubility Increase at the Main Absorption Site on Bioavailability of BCS Class II Drug (Risperidone) Using Liquisolid Technique. *Drug Deliv.* **2017**, *24*, 328–338. [CrossRef]
39. Gattefossé. *Transcuto*$^{l®}$ *P For Efficient Drug Solubilization and Skin Penetration*; Gattefossé: Saint-Priesr Cedex, France, 2020; pp. 1–24. Available online: https://www.gattefosse.com/pharmaceuticals-products/transcutol-p (accessed on 29 April 2023).
40. Salimi, M.; Fouladi, A. Effect of the Various Penetration Enhancers on the *In vitro* Skin Permeation of Meloxicam through Whole Rat Skin. *Eur. J. Bio. Pharm. Sci* **2015**, *2*, 1282–1291.
41. Sullivan, D.W.; Gad, S.C.; Julien, M. A Review of the Nonclinical Safety of Transcutol Ò, a Highly Purified Form of Diethylene Glycol Monoethyl Ether (DEGEE) Used as a Pharmaceutical Excipient. *Food Chem. Toxicol.* **2014**, *72*, 40–50. [CrossRef]
42. Zirak, M.B.; Pezeshki, A. Effect of Surfactant Concentration on the Particle Size, Stability and Potential Zeta of Beta Carotene Nano Lipid Carrier. *Int. J. Curr. Microbiol. Appl. Sci.* **2015**, *4*, 924–932.
43. Softisan. Available online: www.warnergraham.com/images/SoftisanHardFatsProdIn.pdf (accessed on 10 February 2022).
44. Available online: https://pubchem.ncbi.nlm.nih.gov/compound/Glyceryl-behenate (accessed on 10 February 2022).
45. Gycerol Dibehenate. *European Pharmacopeia*; Conseil de l'Europe: Strasbourg, French, 2007; pp. 2110–2111.
46. Cirri, M.; Mennini, N.; Maestrelli, F.; Mura, P.; Ghelardini, C.; Di Cesare Mannelli, L. Development and *In Vivo* Evaluation of an Innovative "Hydrochlorothiazide-in Cyclodextrins-in Solid Lipid Nanoparticles" Formulation with Sustained Release and Enhanced Oral Bioavailability for Potential Hypertension Treatment in Pediatrics. *Int. J. Pharm.* **2017**, *521*, 73–83. [CrossRef]
47. Radomska-Soukharev, A.; Muller, R.H. Chemical Stability of Lipid Excipients in SLN-Production of Test Formulations, Characterization and Short-Term Stability. *Pharmazie* **2006**, *61*, 425–430.
48. Tan, S.F.; Masoumi, H.R.F.; Karjiban, R.A.; Stanslas, J.; Kirby, B.P.; Basri, M.; Basri, H.B. Ultrasonic Emulsification of Parenteral Valproic Acid-Loaded Nanoemulsion with Response Surface Methodology and Evaluation of Its Stability. *Ultrason. Sonochem.* **2016**, *29*, 299–308. [CrossRef] [PubMed]
49. Tang, S.Y.; Shridharan, P.; Sivakumar, M. Impact of Process Parameters in the Generation of Novel Aspirin Nanoemulsions—Comparative Studies between Ultrasound Cavitation and Microfluidizer. *Ultrason. Sonochem.* **2013**, *20*, 485–497. [CrossRef]
50. Aoki, M.; Ring, T.A.; Haggerty, J.S. Analysis and Modeling of the Ultrasonic Dispersion Technique. *Adv. Ceram. Mater.* **1987**, *2*, 209–212. [CrossRef]
51. Özdemir, S.; Çelik, B.; Üner, M. Properties and Therapeutic Potential of Solid Lipid Nanoparticles and Nanostructured Lipid Carriers as Promising Colloidal Drug Delivery Systems. In *Materials for Biomedical Engineering*; Elsevier: Amsterdam, The Netherlands, 2019; pp. 451–499. [CrossRef]
52. Moghimi, S.M.; Hunter, A.C. Poloxamers and Poloxamines in Nanoparticle Engineering and Experimental Medicine. *Trends Biotechnol.* **2000**, *18*, 2958–2964. [CrossRef] [PubMed]
53. Han, F.; Li, S.; Yin, R.; Liu, H.; Xu, L. Effect of Surfactants on the Formation and Characterization of a New Type of Collodial Drug Delivery System: Nanostructured Lipid Carriers. *Colloids Surfaces A Physicochem. Eng. Asp.* **2008**, *315*, 210–216. [CrossRef]

54. Appasaheb, P.S. A Review on Intranasal Drug Delivery System. *J. Adv. Pharm. Edu. Res.* **2013**, *3*, 333–346.
55. Thorat, S. Formulation and Product Development of Nasal Spray: An Overview. *Sch. J. Appl. Med. Sci.* **2016**, *4*, 2976–2985. [CrossRef]
56. Bunjes, H.; Unruh, T. Characterization of Lipid Nanoparticles by Differential Scanning Calorimetry, X-ray and Neutron Scattering. *Adv. Drug Deliv. Rev.* **2007**, *59*, 379–402. [CrossRef] [PubMed]
57. Garcia-Fuentes, M.; Alonso, M.J.; Torres, D. Design and Characterization of a New Drug Nanocarrier Made from Solid–Liquid Lipid Mixtures. *J. Colloid Interface Sci.* **2005**, *285*, 590–598. [CrossRef] [PubMed]
58. Hu, F.Q.; Jiang, S.-P.; Du, Y.-Z.; Yuan, H.; Ye, Y.Q.; Zeng, S. Preparation and Characterization of Stearic Acid Nanostructured Lipid Carriers by Solvent Diffusion Method in an Aqueous System. *Colloids Surf. B Biointerfaces* **2005**, *45*, 167–173. [CrossRef]
59. Jia, L.-J.; Zhang, D.-R.; Li, Z.-Y.; Feng, F.-F.; Wang, Y.-C.; Dai, W.-T.; Duan, C.-X.; Zhang, Q. Preparation and Characterization of Silybin-Loaded Nanostructured Lipid Carriers. *Drug Deliv.* **2010**, *17*, 11–18. [CrossRef]
60. Boyer, R.F. *Transitions and Relaxations in Amorphous and Semicrystalline Organic Polymers and Copolymers. Encyclopedia of Polymer Science and Technology*; John Wiley & Sons, Inc.: New York, NY, USA, 1977; pp. 745–839.
61. Boutonnet-Fagegaltier, N.; Menegotto, J.; Lamure, A.; Duplaa, H.; Caron, A.; Lacabanne, C.; Bauer, M. Molecular Mobility Study of Amorphous and Crystalline Phases of a Pharmaceutical Product by Thermally Stimulated Current Spectrometry. *J. Pharm. Sci.* **2002**, *91*, 1548–1560. [CrossRef]
62. Brandl, F.; Kastner, F.; Gschwind, R.M.; Blunk, T.; Teßmar, J.; Göpferich, A. Release Kinetics. *J. Control. Release* **2009**, *142*, 221–228. [CrossRef]
63. Marx, D.; Williams, G.; Birkhoff, M. Intranasal Drug Administration—An Attractive Delivery Route for Some Drugs. In *Drug Discovery and Development*; IntechOpen: London, UK, 2015; pp. 1–23. [CrossRef]
64. Basir, R.; Rahiman, S.F.; Hasballah, K.; Chong, W.; Talib, H.; Yam, M.; Jabbarzare, M.; Tie, T.; Othman, F.; Moklas, M.; et al. Plasmodium Berghei ANKA Infection in ICR Mice as a Model of Cerebral Malaria. *Iran. J. Parasitol.* **2012**, *7*, 62–74. [PubMed]